Design and Characterization of a Multisite Fluorescence Energy-Transfer System for Protein Folding Studies: A Steady-State and Time-Resolved Study of Yeast Phosphoglycerate Kinase[†]

M. Pilar Lillo[‡,§] and Joseph M. Beechem*,[‡]

Department of Molecular Physiology and Biophysics, Vanderbilt University, Nashville, Tennessee 37232, and Departamento de Biofísica, Instituto de Química-Física, CSIC, Serrano 119, E-28006 Madrid, Spain

Barbara K. Szpikowska, Mark A. Sherman, and Maria T. Mas*

Division of Biology, Physical Biochemistry Section, Beckman Research Institute of the City of Hope, Duarte, California 91010

ABSTRACT: A multisite distance-based fluorescence resonance energy-transfer assay system was developed for the study of protein folding reactions. Single- and double-cysteine substitution mutagenesis was utilized to place sulfhydryl residues throughout the tertiary structure of the bidomain enzyme yeast phosphoglycerate kinase (PGK). These reactive cysteines were covalently modified with extrinsic donor [5-[[2-(2-iodoacetamido)ethyl]amino]-1-naphthalenesulfonic acid] and acceptor (5-iodoacetamidofluorescein) fluorescent labels. A detailed experimental strategy was followed, which revealed that, when these relatively large extrinsic fluorescent labels are covalently attached to properly selected solvent-exposed residues, they do not affect the intrinsic stability of the protein. The PGK crystal structure was combined with molecular dynamics simulations of the dyes built into the protein and time-resolved anisotropy experiments, in order to estimate a more realistic orientation factor, $\langle\kappa^2\rangle^*$, for each donor/acceptor pair. Time-resolved and steady-state fluorescence energy-transfer experiments revealed that this distance assay, spanning six different donor−acceptor distances, is linear and accurate (to within 10−20%) over the range of 30−70 Å. This distance assay system for PGK allows for the measurement of long-range changes in intra- and interdomain spatial organization during protein folding reactions. The approach which we have developed can be applied to any protein system in which unique one- and two-site cysteine residues can be engineered into a protein. In the following paper [Lillo, M. P., et al. (1997) *Biochemistry 36*, 11273−11281], these multisite energy-transfer pairs are utilized for stopped-flow unfolding studies.

The use of fluorescence spectroscopy to study protein folding kinetics has had a very long and successful history. This success stemmed primarily from the fact that fluorescence signals are often very sensitive to the folded state of proteins and measurements can be made with good intrinsic timing resolution. With this extreme sensitivity, fluorescence folding studies have generated an abundance of high-quality data with complex multiphasic kinetic patterns. One serious problem, however, has plagued all of these studies. How was one to interpret this complex change in (typically) an integrated total-intensity signal in terms of fundamental physical properties associated with folding intermediates? Given a simple steady-state fluorescence signal, no fundamental interpretation is really possible. Therefore, application of fluorescence spectroscopy to the protein folding problem was in a fundamental conundrum. What was the use of being able to measure a fluorescence signal change with high accuracy and timing resolution if you cannot interpret the observed signal changes in terms of any fundamental property of the folding intermediates?

The goal of the experiments described in this study was to develop a fluorescence assay for protein folding in which the signal changes could be directly translated into changes in intramolecular distances. To achieve this goal, a multisite fluorescence energy-transfer capability was engineered into a single-protein system, yeast phosphoglycerate kinase (PGK),[1] using cysteine substitution mutagenesis. Due to many intrinsic problems associated with performing fluorescence energy-transfer measurements, extra precautions were taken in order to ensure that the "optical distance" assay was working properly. For each pair of donor/acceptor sites, a maximum of nine mutant proteins were examined, in terms of both biological stability/activity and photophysical properties. This highly developed energy-transfer distance assay system for PGK has the potential for illuminating aspects

[1] Abbreviations: D-PGK, donor-labeled protein; D-PGK-A, donor- and acceptor-labeled protein; CM, center of mass of the emission spectrum; FRET, Förster resonance energy transfer; fwhm, full width at half-maximum probability; IAEDANS, 5-[[[(2-iodoacetyl)amino]ethyl]amino]naphthalenesulfonic acid; AEDANS, reacted IAEDANS covalently attached to protein; IAF, 5-iodoacetamidofluorescein; AF, reacted IAF covalently attached to protein; GuHCl, guanidine hydrochloride; MD, molecular dynamic; MOPS, 3-(*N*-morpholino)propanesulfonic acid; HEPES, *N*-(2-hydroxyethyl)piperazine-*N*′-2-ethanesulfonic acid; EDTA, ethylenediaminetetraacetic acid; DTT, DL-dithiothreitol; PGK, phosphoglycerate kinase from *Saccharomyces cerevisiae*; Trp, tryptophan; $\langle\kappa^2\rangle^*$, orientation factor which takes into account protein crystal structure, steric constraints, and measured rotational dynamics of the dyes.

of the protein folding problem which may not be obtainable in any other manner (e.g., real-time measurement of long-range changes in intra- and interdomain organization). The approach which we have developed can be applied to any protein system in which unique one- and two-site cysteine residues can be engineered into a protein.

MATERIALS AND METHODS

1,5-IAEDANS and 5-IAF were purchased from Molecular Probes, Inc. (Eugene, OR). DE-52 cellulose was from Whatman (Hillsboro, MA) and Ultrogel AcA202 from IBF Biotechnics (Columbia, MD). MOPS, HEPES, DTT, and substrates for PGK activity assays were from Sigma Chemical Co. (St. Louis, MO). Guanidine hydrochloride (sequanal grade) was from Pierce (Rockford, IL). The protein assay kit was purchased from Bio-Rad Labs (Hercules, CA), and Centricon-30 microconcentrators were purchased from Amicon, Inc. (Beverly, MA).

Protein Purification and Characterization. Single- and double-cysteine mutants of yeast PGK were constructed using site-specific mutagenesis of yeast PGK cDNA in which the single cysteine at position 97 had been previously mutated to a serine, C97S (Sherman et al., 1990; Haran et al., 1992). In addition to two single-cysteine mutants, Q135C and S290C, and a double-cysteine mutant, Q135C/S290C, which were described previously (Haran et al., 1992), three additional single-cysteine mutants, S75C, T202C, and S412C, and five double-cysteine mutants, Q135C/S412C, S75C/S412C, T202C/S412C, S75C/S290C, and S290C/S412C, were constructed for this study. Each mutated gene was sequenced to confirm the presence of only the desired mutations (Chen & Seeburg, 1985).

PGK mutants were expressed in the *Saccharomyces cerevisiae* XSB44-35D strain, which lacks PGK, and purified as previously described (Haran et al., 1992). Specific activities of the mutants were determined as described previously (Mas et al., 1986). Concentrations of unlabeled proteins were determined spectrophotometrically at 280 nm, using an absorbance for a 1 mg/mL solution of 0.49, determined for wild-type (WT) PGK using the method of Gill and von Hippel (1989). Specific activities of the single- and double-cysteine mutants were within the range of the specific activities of WT PGK preparations.

Protein Labeling with IAEDANS and IAF. Covalent modification of single-cysteine mutants with IAEDANS and/or IAF was carried out as described previously (Haran et al., 1992), with several modifications. Protein samples (2−3 mg/mL) in 50 mM HEPES buffer (pH 8.0) and 1 mM EDTA were incubated at 4 °C for 1 h with a 20-fold molar excess of IAEDANS or for 4 h with a 40-fold molar excess of IAF. The reactions were carried out in the dark, with magnetic stirring. A 10-fold molar excess (over probe concentration) of DTT was added, and incubation was continued for 1 h to terminate the protein modification reaction. The labeled samples were separated from free probes by gel filtration on an Ultrogel AcA202 column, equilibrated with the above buffer containing 1 mM DTT. For samples labeled with IAF, extensive dialysis against the same buffer was necessary following the column filtration step to completely remove free IAF.

Modification of double-cysteine (Cys-PGK-Cys) mutants was carried out in two steps. First, the sample was incubated with IAEDANS under conditions which led to partial labeling. The resulting reaction mixture contained unlabeled PGK (Cys-PGK-Cys) and singly labeled, Cys-PGK-D and D-PGK-Cys, and doubly labeled protein, D-PGK-D. The conditions of the chemical modification were the same as those for the single-cysteine mutants described above, except for the incubation time, which was reduced from 1 h to 20 min. The species with one cysteine labeled with AEDANS and the second cysteine free (D-PGK-Cys and/or Cys-PGK-D) were separated from the other components using an anion exchange DE-52 cellulose (Whatman, Hillsboro, OR) column (12 × 1.5 cm) equilibrated with 10 mM MOPS (pH 7.5) and 1 mM EDTA at 4 °C (see Results and Discussion) and then labeled with IAF to obtain doubly labeled species (D-PGK-A and A-PGK-D). The labeling of D-PGK-Cys with IAF was performed in 10 mM MOPS buffer (pH 7.5) containing 1 mM EDTA and 1 mM DTT, as described above for single-cysteine mutants.

The protein concentration before labeling was determined spectrophotometrically at 280 nm, as described above. Concentrations of labeled protein samples were determined by the method of Bradford (1976), using wild-type PGK to prepare standard curves. After the first step, the specific activities of the labeled PGK mutants were decreased by 10−15% compared to those of the unlabeled proteins, and by an additional 10−15% following the second reaction step. The net activity loss for the final samples was similar to the activity loss experienced by WT PGK when subjected to identical procedures (25−30%). The stability of the labeled samples was not significantly changed (see Results and Discussion).

The extent of labeling with IAEDANS and IAF was determined spectrophotometrically, using molar extinction coefficients of 4300 M^{-1} cm^{-1} (±450) at 337 nm and 61 000 M^{-1} cm^{-1} (±4000) at 492 nm, respectively. These extinction coefficients (and their corresponding error estimates) represent the average extinction coefficients of PGK-bound AEDANS and AF determined spectrophotometrically for several ($n \approx 25$) pure preparations of single- and double-cysteine mutants covalently labeled with each probe. Centricon-30 microconcentrators were used to concentrate protein samples and to exchange buffer to 50 mM MOPS (pH 7.5) containing 100 mM NaCl and 1 mM DTT, for the fluorescence measurements.

Steady-State Fluorescence Emission Spectra. Corrected steady-state emission spectra were obtained with a SPEX 1681 Fluorolog spectrofluorometer (Edison, NJ), equipped with a 450 W xenon arc lamp. AEDANS and AF fluorescence emission were collected from 400 to 700 nm by exciting the donor and donor- and acceptor-labeled proteins at 340 nm. Acceptor emission was collected from 465 to 700 nm, by exciting directly AF at 440 or 460 nm in the donor/acceptor samples. Tryptophan emission spectra were excited at 295 nm, with emission collected from 300 to 410 nm. The excitation and emission band width were 1−2 nm for all the spectra. Background fluorescence from unlabeled protein, buffer, and denaturant was recorded and subtracted from the protein spectra.

Steady-state measurements were performed in a 150 μL fluorescence cuvette with 10 mm (excitation) and 2 mm (emission) path lengths. The absorbance at the excitation wavelength was always lower than 0.03 (10 mm path length), and the absorbance at the maximum of the absorption spectra

of fluorescein in the donor/acceptor samples was lower than 0.1. The temperature of the measurements was 25 ± 0.1 °C.

Time-Resolved Fluorescence Measurements. Time-resolved fluorescence measurements were performed using a frequency-doubled Coherent Antares Nd:YAG laser (Palo Alto, CA) synchronously pumping a dye laser (Coherent 702) using kiton red (Exiton, Dayton, OH) for AEDANS and AF at 325 nm. A laser repetition rate of 4 MHz was utilized, and the pulse width was approximately 1 ps. A half-wave plate in the excitation beam was utilized to rotate the excitation polarization to horizontal for the determination of the polarization bias (*G* factor) of the detection instrumentation. The fluorescence emission signal was passed through a Glan-Thompson polarizer and a Hoya (Fremont, CA) 420 cut-on filter and focused into a SPEX 0.22 m emission monochromator set at 450 nm (donor emission studies) or 560 nm (acceptor emission studies), with a band width of $2-4$ nm, and detected by a 6 μm microchannel plate detector (Hamamatsu R2809U-01, Bridgewater, NJ) operating in the single-photon-counting, time-correlated mode (Bloom et al., 1994; Jones et al., 1995). The impulse response functions were typically $40-80$ ps at fwhm. Timing calibration was $6-12$ ps/channel, with $5000-8000$ channels of data obtained. Typical total intensity sum curves had approximately 10 000 counts in the peak channel ($\approx 30 \times 10^6$ total photons). Time-resolved measurements were performed on 120 μL samples in cuvettes with a 3×3 mm path length. Protein solutions ($1-4$ μM) were prepared in 50 mM MOPS, 100 mM NaCl, 1 mM EDTA, and 1 mM DTT, at pH 7.5. The temperature of the measurements was 25 ± 0.2 °C. During acquisitions, the emission polarizer rotated from vertical to horizontal every 30 s to measure the parallel ($\parallel$) and perpendicular ($\perp$) components of the emission. The thermostated sample holder was rotated from the donor-only cuvette to the donor/acceptor cuvette every 60 s (ISS Koala unit, Urbana, IL).

Data Analysis. Time-resolved fluorescence anisotropy decays were used to study internal rotational motions of the probes attached to the protein. Simultaneous analyses of the parallel and perpendicular intensity decays were performed using Globals Unlimited (Urbana, IL) as described in Beechem et al. (1991). Anisotropy decays, $r(t)$, were found to be adequately described as a biexponential function:

$$r(t) = \beta_f \exp(-t/\phi_f) + \beta_g \exp(-t/\phi_g) \qquad (1)$$

where β_f and β_g are the amplitudes of the fast local probe motion (ϕ_f) and overall global protein motion (ϕ_g), respectively. Within the context of an orientation factor calculation (see below), β_g represents the limiting anisotropy (i.e., the long-time asymptote) for the fast local motion of the probe (β_f). A nonassociative anisotropy decay model [e.g., Beechem et al. (1991)] was utilized for all of the labeled proteins. The goodness of the fit was judged by examination of randomness in the residual distribution and recovered global χ square (χ_g^2).

Equilibrium Unfolding Studies Monitored by Steady-State Fluorescence. All of the site-specific energy-transfer pairs have been designed in order to examine changes in distances during equilibrium and kinetic folding studies. Since experiments need to be performed under both native and unfolded conditions, the number (and importance) of the "donor-only" controls are crucial for obtaining meaningful energy-transfer

results. Since the final resonance energy-transfer efficiencies are calculated as the ratio of two different protein samples (donor-only and donor/acceptor pair), one has to ensure that both samples have identical (or nearly identical) stabilities. The unfolding transitions for D-PGK and D-PGK-A samples were monitored using fluorescence (steady-state and time-resolved) techniques with guanidinium hydrochloride (Gu-HCl) as a denaturant.

For some measurements, it was found useful to quantitate folding transitions using the measured center of mass, CM (eq 2), of the emission spectra:

$$CM = \frac{\sum \lambda_i F(\lambda_i)}{\sum F(\lambda_i)} \qquad (2)$$

where $F(\lambda_i)$ is the fluorescence intensity measured at the emission wavelength λ_i. Changes in the center of mass of the emission spectra as well as fluorescence total intensity of AEDANS in D-PGK ($\lambda_{ex} = 340$ nm), AF in D-PGK-A ($\lambda_{ex} = 460$ nm), and tryptophan ($\lambda_{ex} = 295$ nm) in both D-PGK and D-PGK-A samples were utilized to monitor guanidine-induced transitions. Unfolding transitions were also examined using the energy-transfer efficiencies.

The protein samples (series of protein solutions at identical protein concentration) were incubated at each GuHCl concentration (from 0 to 2 M) for a minimum of 3 h prior to measurement to assure that equilibrium conditions had been reached [the proteins are completely unfolded at 2 M GuHCl (Szpikowska et al., 1994)]. The GuHCl concentration of the stock solutions was determined using the refractive index of Pace et al. (1989) and an empirical equation (Nozaki, 1972). Folding reversibility of all the labeled PGK samples was examined by dilution of the unfolded samples from 1.5 to 0.15 M GuHCl (MOPS buffer). All the preparations contained 1 mM DTT.

The transition midpoints and cooperativity indexes were calculated by fitting the experimental data (using a nonlinear least-squares algorithm, Sigma Plot software, San Rafael, CA) to the equation derived from the denaturant binding model as described by Szpikowska et al. (1994). This method of analysis was selected to allow for a direct comparison of the stability measured for wild-type PGK and those of all the variously labeled mutants.

The unfolding curves were normalized to the apparent fraction of the unfolded form:

$$F(U) = (Y_{obs} - Y_F)/(Y_U - Y_F) \qquad (3)$$

where Y_{obs} is the observed physical parameter (fluorescence) at a given denaturant concentration and Y_F and Y_U are values of the Y characteristic of the folded and unfolded conformations, respectively, at the same denaturant concentration.

The baseline correction was done, prior to normalization, using linear extrapolation of the baselines in the pre- and post-transition regions to obtain estimates of Y_F and Y_U in the transition region (Pace et al., 1989; Szpikowska et al., 1994).

Measurements of Energy Transfer. The Förster distance, R_o, is the dye-to-dye separation distance for 50% efficiency of resonance energy transfer. This constant is calculated (in angstroms) using the spectroscopic properties of the donor and acceptor:

$$R_o = 0.211(n^{-4}Q_D\kappa^2 J)^{1/6} \tag{4}$$

A refractive index (n) of 1.4 was used for all protein samples ($n_{BUFFER} = 1.337$, $n_{2MGuHCl} = 1.375$, and $n_{PROTEIN} \sim 1.4$). The fluorescence quantum yield of the donor samples (Q_D) was determined for each position by reference to a solution of quinine bisulfate in 0.1 N H_2SO_4, using a quantum yield for quinine of 0.51 (Velapoldi, 1972). J (M^{-1} cm^{-1} nm^4) is the spectral overlap integral between the emission spectrum of the donor and the absorption spectrum of the acceptor and was approximated by

$$J = [\sum F_D(\lambda)\epsilon_A(\lambda)\lambda^4\Delta\lambda]/[\sum F_D(\lambda)\Delta\lambda] \tag{5}$$

where $F_D(\lambda)$ was the corrected emission spectrum of the donor-labeled samples (arbitrary units) and $\epsilon_A(\lambda)$ the extinction coefficient (M^{-1} cm^{-1}) of the acceptor from the donor/acceptor samples. Acceptor extinction coefficients at $\lambda = 492$ nm were determined for all the different labeled preparations and found to be nearly identical ($\epsilon^{492} = 61\,000$ M^{-1} cm^{-1}).

The orientation factor (κ^2) depends on the relative orientation of the transition dipoles of the donor and acceptor. In the samples described in this work, multiple estimations of the orientation factor were performed. The first estimation was to calculate the Förster distance R_o, introducing into eq 4 the isotropic dynamic average value of κ^2 ($\kappa^2 = 2/3$; Dale & Eisinger, 1975). In addition, steady-state and time-resolved fluorescence anisotropies of all the labeled samples were examined in order to obtain a more realistic estimation of the proper orientational averaging. From the measured limiting anisotropy for the fast local motion (β_g) (refer to eq 1), the donor and acceptor depolarization factors $\langle d_D^x \rangle$ and $\langle d_A^x \rangle$ were calculated as $\langle d_i^x \rangle = (\beta_g/r_f)^{1/2}$ (Soleillet's theorem; Dale et al., 1979). The half-cone angle, θ_c, over which the probes move, was also estimated using $(\beta_g/r_f)^{1/2} = \cos\theta_c(1 + \cos\theta_c)/2$ (hindered rotation model; Kinosita et al., 1977). The measured anisotropy value at time zero (i.e., $\beta_g + \beta_f$, eq 1) was found to match the fundamental anisotropy (r_f) previously reported for both of these probes (donor $r_f = 0.20 \pm 0.02$, acceptor $r_f = -0.14 \pm 0.02$) (Hudson & Weber, 1973; Chen & Bowman, 1965). Applying averaging analysis, we estimated the maximum and minimum $\langle \kappa^2 \rangle$ values (eqs 6 and 7) from the measured depolarization factors (Dale el al., 1979):

$$\langle \kappa^2 \rangle_{max} = 2/3(1 + \langle d_D^x \rangle + \langle d_A^x \rangle + 3\langle d_D^x \rangle\langle d_A^x \rangle) \tag{6}$$

$$\langle \kappa^2 \rangle_{min} = 2/3[1 - (\langle d_D^x \rangle + \langle d_A^x \rangle)/2] \tag{7}$$

R_o^{max} and R_o^{min} are the Förster distances derived from the minimum and maximum values of κ^2 from the relationship $R_o^{max/min} = (1.5\langle\kappa^2\rangle^{max/min})^{1/6}R_o(2/3)$. For the unfolded samples, depolarization of the fluorescence anisotropy was essentially complete before emission (see Table 3), allowing the use of $\kappa^2 = 2/3$.

Looking for a Better Estimation of $\langle \kappa^2 \rangle^*$. The above $\langle \kappa^2 \rangle$ (min/max) calculation, however, does not make use of the crystal structure of PGK and the known site locations of the inserted cysteines. For instance, the $\langle \kappa^2 \rangle$ (min/max) calculation above would allow the dye probe to sample conformations which would clearly not be allowed due to simple steric constraints. To obtain a $\langle \kappa^2 \rangle$ calculation which was consistent

with the known crystal structure, the donor and acceptor probes were built into the crystal structure (Brookhaven Protein Data Bank file 3PGK; Watson et al., 1982) so that a "sterically appropriate" orientational averaging could be performed. For the serine → cysteine mutants (S75C, S290C, and S412C), it was relatively easy to replace the serine OH with the cysteine SH, maintaining the same geometry as in the crystal structure. The probe label was then built onto the SH as S-CH$_2$-CO-NH-fluorescein or S-CH$_2$-CO-NH-CH$_2$-CH$_2$-NH-naphthalene-1-sulfonic acid. For Q135C, the glutamine side chain was replaced with cysteine so that the sulfur atom assumed the position of the glutamine C-γ atom. For T202C, the threonine side chain was replaced with cysteine so that the sulfur atom assumed the position of the threonine O-γ atom. Molecular models of AF and AEDANS were constructed from fragments supplied with BIOGRAF (Molecular Simulations Inc., Waltham, MA) and energy minimized using the DREIDING II force field (Mayo et al., 1990). The region of conformational space accessible to each probe was evaluated by dynamics simulation in which four torsion angles (bonds connecting C-α, C-β, S-γ, probe methylene C, and probe carbonyl C) were allowed to vary randomly and simultaneously (Monte Carlo simulation). Of the 500 conformers generated, those with the lowest energy were saved ($\approx$100 conformers) and their coordinates averaged to generate an estimate of the equilibrium configuration of the emission oscillator for the donor and the absorption oscillator for the acceptor. The MD calculations allowed all but the sterically restricted configurations of the probes to be adopted. In theory, the MD simulations could have been utilized to obtain not only the "mean configuration" of the probe but also the full $\langle \kappa^2 \rangle$ by calculating depolarization factors from the individual MD trajectories. However, it was felt that the measured time-resolved anisotropy provided a much more accurate measurement of the probe's motion. Therefore, the mean probe configuration from MD was combined with the measured time-resolved anisotropy of the probes motion to obtain a final formula for $\langle \kappa^2 \rangle^*$:

$$\langle \kappa^2 \rangle^* = MD(\theta_D, \theta_A, \psi)\langle d_D^x \rangle\langle d_A^x \rangle + 1/3(1 - \langle d_D^x \rangle) + 1/3(1 - \langle d_A^x \rangle) + \cos^2(\theta_D)\langle d_D^x \rangle(1 - \langle d_A^x \rangle) + \cos^2(\theta_A)\langle d_A^x \rangle(1 - \langle d_D^x \rangle) \tag{8}$$

where

$$MD(\theta_D, \theta_A, \psi) = [\sin(\theta_D)\sin(\theta_A)\cos(\psi) - 2\cos(\theta_D)\cos(\theta_A)]^2 \tag{9}$$

and θ_D, θ_A, and ψ represent the MD-determined average angular position of the donor and acceptor dipoles and the azimuthal angle connecting the two, respectively [see Dale et al. 1979] and $\langle d_D^x \rangle$ and $\langle d_A^x \rangle$ are the measured depolarization factors from the fluorescence anisotropy decay (see above). It is interesting to note that the MD simulations revealed the same trend in rotational mobility as that measured by the time-resolved anisotropy.

Steady-State Energy Transfer. The ratio of steady-state fluorescence intensities for the donor only (I_D) and the donor in the presence of the acceptor (I_{DA}) (for identical protein concentrations of D-PGK and D-PGK-A, $\lambda_{ex} = 340$ nm, $\lambda_{em} = 400-460$ nm) is proportional to the average energy-

transfer efficiency, $\langle E \rangle$, as described by eq 10:

$$\langle E \rangle = 1 - \frac{I_{DA}}{I_D} \tag{10}$$

Two labeled samples, D-PGK and D-PGK-A, were used for each set of experiments. The transfer efficiency was also calculated from sensitized acceptor emission.

The measured energy-transfer efficiency was used to calculate the average distance, $\langle R \rangle$, between the donor and acceptor transition dipoles by using eq 11:

$$\langle R \rangle = R_o \left(\frac{1 - \langle E \rangle}{\langle E \rangle} \right)^{1/6} \tag{11}$$

Time-Resolved Energy Transfer (Empirical Exponential Analysis). Determination of the average energy-transfer efficiencies, $\langle E \rangle$, was also obtained from the ratio of the average lifetimes of the D-PGK, $\langle \tau_D \rangle$, and D-PGK-A, $\langle \tau_{DA} \rangle$, calculated from a nonlinear least-squares multiexponential fitting procedure:

$$I_D(t) = \sum \alpha_i \exp(-t/\tau_{D_i}) \tag{12}$$

The average donor lifetime, $\langle \tau_D \rangle$, is calculated with the equation

$$\langle \tau_D \rangle = \sum_{i=1}^{n} \alpha_i \tau_{D_i} / \sum_{i=1}^{n} \alpha_i \tag{13}$$

α_i and τ_{D_i} are the amplitude and lifetime, respectively of the *i*th component. Three lifetimes are required for adequate fitting for the donor-only samples at $\lambda_{em} = 450$ nm, and two lifetimes are required at $\lambda_{em} = 560$ nm. The fluorescence decay of the donor/acceptor pair was also empirically analyzed by multiexponentials. This analysis gave the average $\langle \tau_{D(A)} \rangle$. The average energy-transfer efficiency was calculated by $\langle E \rangle = 1 - \langle \tau_{D(A)} \rangle / \langle \tau_D \rangle$. Since $\langle \tau_{D(A)} \rangle$ and $\langle \tau_D \rangle$ are obtained without the need of absolute protein concentrations, uncertainties associated with protein concentration determination are eliminated by the time-resolved fluorescence measurements.

Time-Resolved Distance Analyses. Discrete donor−acceptor distances were also obtained from direct simultaneous analysis of both the donor-only and donor/acceptor decays using

$$I_{D(A)}(t) = \sum_{i=1}^{n} \alpha_i \exp \left[-t \left[\frac{1}{\tau_{D_i}} + \frac{1}{\tau_{D_i}} \left(\frac{R_o}{R} \right)^6 \right] \right] \tag{14}$$

If the protein has conformational flexibility in solution, the interchromophoric distance will not be unique, and eq 14 will not be able to adequately represent the measured data. The observed donor decay in the presence of the acceptor will contain multiple contributions with a probability distribution function dependent upon the distribution of D−A distances, $P(R)$ (Haas et al., 1978, 1988; Haas & Steinberg, 1984):

$$I_{D(A)} = \int_0^{R_m} P(R) \sum_{i=1}^{n} \alpha_i \exp \left[-t \left[\frac{1}{\tau_{D_i}} + \frac{1}{\tau_{D_i}} \left(\frac{R_o}{R} \right)^6 \right] \right] dR \tag{15}$$
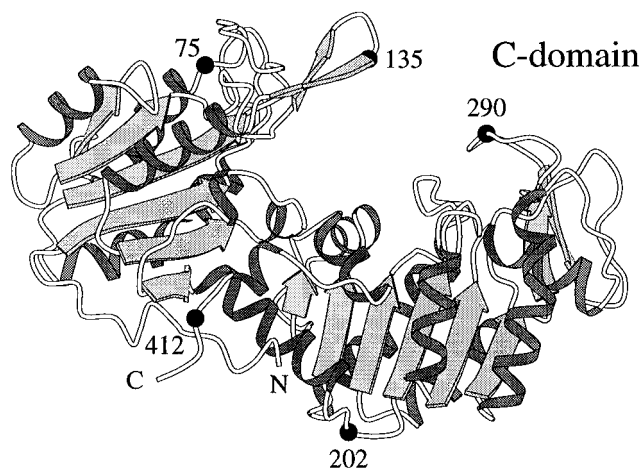

FIGURE 1: Schematic representation of the crystal structure of yeast PGK (Brookhaven Protein Data Bank file 3PGK), showing the position of the residues that were modified (●). Of the six distances measured in this study, the 135 ↔ 290, 75 ↔ 290, 290 ↔ 412, and 412 → 202 are interdomain distances and 135 ↔ 412 and 412 → 75 are intradomain distances. Residue 412 is only three residues apart from the C-terminal end, and it is situated on the N-terminal domain in the folded protein.

R_m is the maximum D−A distance. In this study, we used a Gaussian form for the distribution $P(R)$ to describe the shape of the distance distribution:

$$P(R) = \frac{1}{\sigma\sqrt{2\pi}} \exp \left[-\frac{(R - R_c)^2}{2\sigma^2} \right] \tag{16}$$

where R is the D−A distance, R_c is the mean distance of the calculated distribution (most probable distance), and σ is the standard deviation of the distribution. We did not attempt to resolve the intrasite diffusion coefficient in these analyses (Haas & Beechem, 1989). In these global analyses, the donor-only lifetimes, τ_{D_i}, were linked between both D-PGK and D-PGK-A decay curves. It was found that all of the observed dynamic quenching could be adequately represented (see Figure 3 for a typical fit) using only the energy-transfer distance terms. R_c and σ were adjustable parameters in the fitting of the donor/acceptor decay data. The χ_g^2 and residuals distribution were utilized to judge the goodness of the fit.

RESULTS AND DISCUSSION

The locations of the cysteines engineered into PGK are shown in Figure 1. The overall design concept is the generation of unique fluorescence labeling sites by replacement of one or two selected residues with a cysteine. In this work, an initial set of six different energy-transfer pairs was characterized in terms of both site-specific photophysical properties and enzyme stability. Although it is possible (in theory) to make an energy-transfer measurement with only two labeled protein samples (donor only and donor/acceptor pair), we decided to take a more rigorous approach to characterizing the energy-transfer pairs in this system. To generate a completely defined "distance assay" between any single site on PGK, as many as nine proteins were examined. This experimental design strategy included a range of extra controls which are important when using fluorescence

Table 1: Summary of the Labeled Proteins Examined for the Photophysical Characterization of Each Energy-Transfer Pair Cys$i$ → Cys$j$

sample	name	Cys$i$ → Cys$j$	no. of cysteines	fluorophore
donor only (D-PGK)	i-single cysteine	D- - -	1 (i)	AEDANS (i)
	j-single cysteine	- - -D	1 (j)	AEDANS (j)
	i-two cysteines	D- - -Cys	2 (i, j)	AEDANS (i)
	j-two cysteines	Cys- - -D	2 (i, j)	AEDANS (j)
	(i, j)-two cysteine average	D- - -Cys + Cys- - -D	2 (i, j)	AEDANS (i) + AEDANS (j)
	(i, j)-two cysteine "double donor"	D- - -D	2 (i, j)	AEDANS (i, j)
acceptor only	i-single cysteine	A- - -	1 (i)	AF (i)
	j-single cysteine	- - -A	1 (j)	AF (j)
donor-acceptor (D-PGK-A)	i, j specific label	D → A	2 (i, j)	AEDANS (i) and AF (j)
	j, i specific label	A ← D	2 (i, j)	AEDANS (j) and AF (i)
	i, j average label	D → A + A ← D	2 (i, j)	AEDANS (i) and AF (j) and + AEDANS (j) and AF (i)

energy transfer to monitor protein folding reactions. Table 1 summarizes the various modified proteins which have been examined for each energy-transfer pair. It is important to understand the symbols in Table 1. For instance, fluorescence energy transfer between sites i and j requires cysteines at both the i and j sites. To "force" the donor label (IAEDANS) exclusively to site i, the single-cysteine mutant is examined. Similarly, to force the donor to site j, the single-cysteine mutant at site j is examined. These single-site mutants are extremely useful in unequivocally characterizing the photophysical characteristics of each individual labeling site (i.e., rotational mobility, lifetimes, emission spectra, etc.). These single-site mutants, however, are not particularly well suited for serving as donor-only or acceptor-only controls because the double-cysteine mutants must be used for all of the actual fluorescence energy-transfer measurements. Therefore, additional spectroscopic studies were performed on the double-cysteine mutants.

In order to be able to individually characterize the various labeled protein species in the double-cysteine mutants, it is important to be able to chemically separate each labeled species (refer to the multiple two-cysteine-labeled proteins in Table 1). For the labeled PGK proteins, it was possible to separate many (in some cases all) of the singly and doubly labeled proteins from each other. For the double-cysteine-containing proteins, a two-stage reaction and purification procedure was utilized.

Reaction with IAEDANS (donor) generates a total of four protein species: Cys-PGK-Cys (unlabeled protein), D-PGK-Cys, Cys-PGK-D, and D-PGK-D. To separate these multiple labeled species, anion exchange chromatography was utilized. Figure 2A depicts a chromatographic profile for the double-cysteine mutant Cys135/Cys412, obtained from the initial reaction mixture with IAEDANS. The peaks in this elution profile were identified by comparing their elution with the elution of the controls: single-cysteine mutants specifically labeled at each site, the unlabeled protein, and the exhaustively labeled double-cysteine mutant. Peaks I and III (Figure 2A) were identified as the unlabeled and doubly labeled proteins, respectively, and peaks IIA and IIB represented D-PGK-Cys412 and Cys135-PGK-D, respectively. Being able to isolate each of the singly labeled donor species (in this case) allowed the measurement of distances from both the specific and the average donor/acceptor labeling positions (see Table 1). The extent of separation of two singly labeled species (D-PGK-Cys and Cys-PGK-D) depends on the location of the probe. The elution volume for the singly labeled mutants (peak I) increases in the following order: C75 < C135 < C202 < C290 < C412.
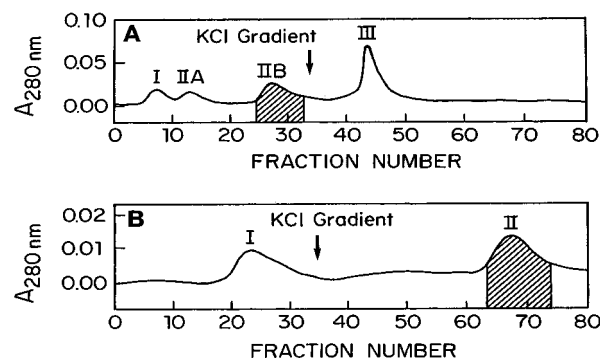

FIGURE 2: Chromatographic separation of D-PGK and D-PGK-A for the C135−C412 mutant. Double-cysteine mutants were labeled with IAEDANS (D) and IAF (A) in a two-step procedure as described in the Materials and Methods. Labeled proteins were separated on a DE-52 cellulose column (12 × 1.5 cm) with a linear salt gradient (0 → 0.25 M KCl). Two milliliter fractions were collected at a flow rate of 20 mL/h. Shown in panel A is the separation of the mixture of labeled and unlabeled species following labeling of the C135−C412 PGK mutant with IAEDANS. In this case, the singly D-labeled species modified at positions 135 and 412 eluted as separate peaks (peaks IIA and IIB, respectively). Peaks I and III represent unlabeled and doubly labeled protein, respectively. In some experiments, peaks IIA and IIB were pooled together prior to IAF labeling. In one experiment, only the 412−135 mutant labeled with AEDANS at C412 (peak IIB in panel A) was subjected to modification with IAF to produce site-specifically labeled protein with D at position 412 and A at position 135 (denoted 412 → 135). Panel B shows separation of D412-PGK-A135 (peak II) from the remaining D412-PGK-SH.

Once the singly labeled donor species were purified, these proteins were further reacted with IAF. Purification of these labeled proteins was much easier, because only two protein species are present: D-PGK-Cys and D-PGK-A. A chromatography profile of the acceptor-reacted protein using peak IIB as starting material (in Figure 2A) is shown in Figure 2B. Comparison with the elution profile of the D-labeled single-cysteine control proteins and examination of the ratio of absorbance at 280 and 492 nm confirmed that peak I was D-PGK-Cys and peak II was D-PGK-A. In all cases, the large chromatographic separation distance between the elution pattern of D-PGK-A and D-PGK-SH protein peaks eliminated any need for spectroscopic corrections associated with incomplete labeling of the D-PGK-SH samples with the acceptor.

This biochemical separation of the various donor/acceptor species allowed for the photophysical characterization of many of the protein species described in Table 1. These samples were also characterized for folding properties (Figure 6 and Table 2) and enzyme activity. Only mutants which

Table 2: Folding Transition Midpoints for All Six D-PGK and D-PGK-A Energy-Transfer Pairs

energy-transfer pair	C_m (M) (tryptophan)[a]	C_m (M) (all)[b]
135 ↔ 290	0.60	0.68
75 ↔ 290	0.53	0.53
135 ↔ 412	0.63	0.63
412 → 135	0.57	0.62
412 → 75	0.59	0.58
290 ↔ 412	0.62	0.62
202 ↔ 412	0.59	0.60
column average	0.59 ± 0.03	0.61 ± 0.05

[a] Center of mass of tryptophan emission spectra of D-PGK and D-PGK-A. [b] From the 0−1 normalized data corresponding to all of the spectroscopic markers described in Figure 5 for D-PGK and D-PGK-A.

could pass all of the required tests, which confirmed their close similarity with respect to WT PGK, were utilized.

The experiments described below demonstrate that all of the characteristic photophysical signatures which indicate energy transfer are apparent for all six of the donor/acceptor pairs described in this study. In all six energy-transfer pairs, one observes (1) a quenching of the donor fluorescence in the presence of acceptor in the native state which decreases dramatically upon unfolding (Figure 3, upper inset), (2) an enhancement of the acceptor fluorescence in the presence of donor in the native state which decreases upon unfolding of the protein (Figure 3, top), (3) a dynamic quench of the fluorescence lifetime of the donor in the presence of acceptor in the native state (Figure 3, bottom) which is greatly diminished upon unfolding, and (4) appearance of characteristic energy-transfer kinetics in the acceptor time-resolved fluorescence which yields essentially identical distances as compared to the donor-emission analysis (Table 5).

A long series of "control-type" experiments will be described first, not in order to establish the existence of fluorescence energy transfer for each pair but rather to determine if there are any unique characteristics associated with any energy-transfer pair which would preclude its use in a real-time kinetic distance assay for protein folding.

Photophysical Characterization of Each Donor-Labeling Site. AEDANS → AF represents perhaps the most utilized fluorescence energy-transfer pair which has been characterized to date (van der Meer et al., 1994). One of the major concerns with using AEDANS as a donor involves the fact that the fluorescence emission is very environment sensitive and multiexponential decay behavior on labeled proteins is often found [e.g., Chantler and Tao (1986)]. The origin of the heterogeneous character of the emission of proteins labeled with IAEDANS is unknown. In this energy-transfer
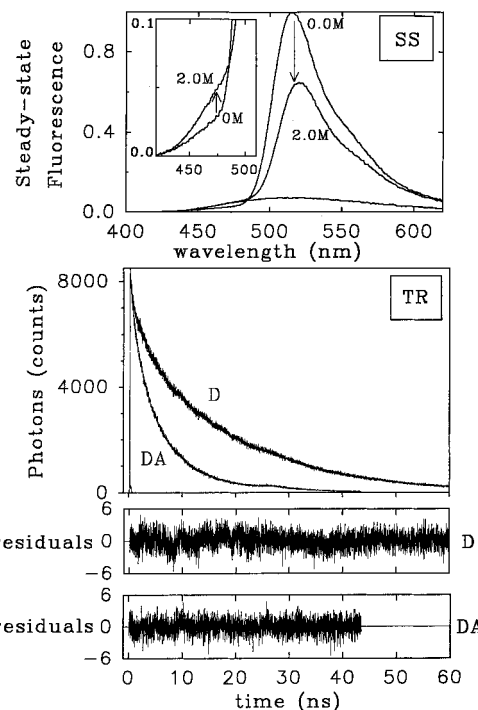

FIGURE 3: Quantitative determination of the origin of the fluorescence changes in the D-PGK-A sample using both steady-state (SS) and time-resolved (TR) fluorescence methodologies. (OMGuHCl, unlabeled spectrum) (SS) Corrected steady-state fluorescence emission spectra of D-PGK and D-PGK-A (135 ↔ 290), folded (0 M GuHCl) and unfolded (2 M GuHCl) proteins, at equal concentrations (2 μM), in MOPS buffer at pH 7.5 and 25 °C, with an λ_{ex} of 340 nm. (Inset) Donor emission increase in D-PGK-A when the protein unfolds. (TR) Time-resolved AEDANS fluorescence total intensity decays for the D-PGK (D) and the D-PGK-A (DA) for the 135 ↔ 412 sample under native conditions (MOPS buffer at pH 7.5 and 0 M GuHCl at 25 °C). The differences between the measured data and the fits from a simultaneous analysis of the donor and donor/acceptor decays (Globals Unlimited, see Materials and Methods) reveal a random residual pattern.

study, the IAEDANS was covalently attached to five different Cys residues of PGK: Cys75, Cys135, Cys202, Cys290, and Cys412. Therefore, it was important to spectroscopically characterize each individual donor-only mutant (in both the native and unfolded states) in terms of (1) quantum yield, (2) emission spectral shape, (3) fluorescence lifetimes, and (4) rotational properties, before labeling the protein with an acceptor fluorophore.

Table 3 summarizes the complete photophysical characterization of AEDANS (donor) labeled at each specific site in PGK. The fluorescence lifetime decay requires three exponentials for all labeled proteins. All sites had a long lifetime term that varied from 14 to 28 ns which accounts

Table 3: Steady-State and Time-Resolved Fluorescence Total-Intensity and Anisotropy Decay Parameters of All the Single-Cysteine D-PGK Samples as a Function of the Labeled Position

donor-only site	Q_f quantum yield (± 0.03)	λ_{em} max (nm)	α_1	τ_1 (ns) (± 0.5)	α_2	τ_2 (ns) (± 0.8)	α_3	τ_3 (ns) (± 0.2)	$\langle r \rangle$ (steady state)	β_g (± 0.02)	ϕ_g (ns) (± 5)	β_f (± 0.03)	ϕ_g (ns) (± 0.3)
290	0.54	496	0.53	27.8	0.26	8.0	0.21	0.5	0.076	0.12	30	0.07	0.6
412	0.40	503	0.63	17.8	0.10	4.6	0.27	0.5	0.081	0.14	23	0.06	0.9
75	0.40	504	0.60	17.9	0.15	5.0	0.25	0.2	0.070	0.12	21	0.10	0.6
135	0.35	513	0.56	15.2	0.18	5.5	0.26	0.6	0.047	0.08	15	0.12	0.6
202	0.36	514	0.42	14.2	0.34	6.5	0.24	0.3	0.053	0.07	18	0.13	0.9
all[a]	0.35	515	0.5	13.5	0.18	4.5	0.32	0.3	0.02	0.06	4 ± 2	0.13	0.6

[a] Unfolded state; β_g and ϕ_g also represent local motion components. Total-intensity (α_i and τ_i) and anisotropy (β_i and ϕ_i) symbols are defined in eqs 12 and 1, respectively.
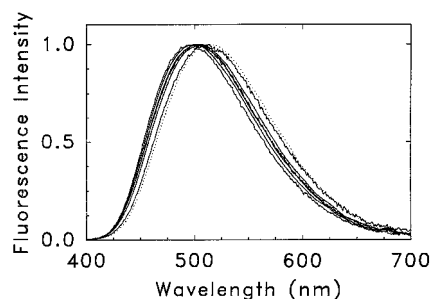
FIGURE 4: AEDANS fluorescence-corrected emission spectra of all six energy-transfer donor-only samples (two-cysteine, single-donor labeled PGK mutants). Proceeding in the order of increasing wavelength of maximum emission: $75 \leftrightarrow 290$, $135 \leftrightarrow 290$, $412 \rightarrow 75$, $135 \leftrightarrow 412$, $290 \leftrightarrow 412$, and $202 \leftrightarrow 412$. MOPS buffer at pH 7.5, where $T = 25$ °C and $\lambda_{ex} = 340$ nm, at 2 μM. The dotted line spectrum represents that observed for all of the unfolded proteins (2 M GuHCl).

for 75–95% of the total fluorescence intensity, a medium lifetime of 5–8 ns, and a short lifetime of 200–600 ps (<1% of total). In the unfolded state, the observed lifetimes for all of the mutant-labeled proteins are identical (within experimental error; see Table 3).

AEDANS bound to Cys135 and Cys202 has properties in the native state which are nearly identical to what is observed for the unfolded protein (see Table 3). These positions have the lowest quantum yield (0.35, similar to the unfolded proteins), the more red-shifted emission spectra ($\lambda_{max} = 512–515$ nm), shorter fluorescence lifetimes, and a less restricted motion (β_f, eq 1) than the probes at other locations. Positions 135 and 202 are absolutely ideal labeling sites, in that as the protein undergoes a folding transition the dye's rotational and photophysical properties are essentially invariant.

AEDANS labeled at Cys290 has the highest quantum yield (0.54), the most blue-shifted emission spectra ($\lambda_{max} = 494$ nm), longest fluorescence lifetimes, and a more restricted rotational environment. Compared to Cys135 and Cys202, Cys290 is in the most protective environmental position of any of our labeled proteins. The photophysical characteristics of Cys412 and Cys75 are between these two extreme classes, but much closer to the unfolded protein state than is Cys290. When the protein unfolds (in the presence of >1 M GuHCl, Table 3 all), the different sites have identical spectroscopic properties.

Although the single-cysteine mutants were very useful for characterization of the individual properties associated with each labeled site, these proteins are not actually utilized in the fluorescence energy-transfer efficiency calculations. For these calculations, the two-cysteine proteins are required. Figure 4 shows the corrected emission spectra of all of the donor-alone (two-Cys mutants), for the native and unfolded state. The emission peak changes from 499 nm for $75 \leftrightarrow 290$ to 513 nm for $202 \leftrightarrow 412$. The unfolded proteins all have an emission maximum of 515 nm. These measured spectral shifts and quantum yield changes were taken into account in the calculation of R_o (see below and Data Analysis). One can see, however, that for these samples the actual spectral changes associated with each particular D–A site are relatively small, generating an average change in overlap integral of only $\approx$8%.

The comparison of the sum of the two emission spectra of each donor single-Cys sample (weighted for the optical density OD at the excitation wavelength) with the OD weighted average emission spectra of the doubly labeled and the singly labeled two-Cys samples (our control in the FRET experiments) allows us to estimate the relative labeling efficiency at each site of the two-Cys mutants and the possible effect of the free cysteine on the fluorescence emission of the donor-only sample. Rather surprisingly, for $135 \leftrightarrow 290$, the two-Cys mutant with the most distinctly different donor-only spectrum, the measured emission spectra of the donor-only two-Cys samples could be exactly represented as the linear combination (50% each) of the emission spectra of the two single-Cys donor-only samples (Cys135 and Cys290). These results reveal that, even under conditions where the cysteine sites are most different in the photophysical environment, the donor probe will be evenly distributed between both sites. It is also clear that the presence of the free Cys in the donor-alone sample has absolutely no effect on the overall fluorescence at the labeled site.

Experiments were also undertaken in order to test whether the presence of two cysteines would affect the intrinsic stability of the protein. PGK's stability can be conveniently monitored using intrinsic tryptophan fluorescence (Szpikowska et al., 1994; Sherman et al., 1995; Beechem et al., 1995). Similar to the unlabeled protein, when the labeled protein unfolds, a large increase in the tryptophan fluorescence is observed and the tryptophan emission spectra are shifted to the red. The advantage of using the tryptophan fluorescence of the labeled protein is that it represents an independent way to study the stability of the D-PGK and D-PGK-A samples. Tryptophan fluorescence emission spectra were found to be identical at 0.0 and 2.0 M GuHCl for both D-PGK and D-PGK-A samples (all mutants), indicating that tryptophan to AEDANS or AF energy transfer in this system must be very small (data not shown). Unfolding experiments were performed on all of the two-Cys mutants, with a special emphasis on examination of the singly labeled and doubly labeled proteins.

In addition to tryptophan fluorescence, it was found that one can monitor the unfolding transition with each of the various fluorescence probes at each site using the emission wavelength shifts in AEDANS and AF (even though these shifts were very small, they were very reproducible and easily quantitated). Figure 5 summarizes the equilibrium unfolding transitions monitored from all the different fluorophores (AEDANS, AF, and Trp, average FRET efficiency). The equilibrium unfolding transitions for all six donor/acceptor proteins followed a simple two-state model (see Figure 5). In Table 2, we compare the C_m determined from the tryptophan emission of the D-PGK and D-PGK-A samples, with the C_m^{all} values from the simultaneous analysis of all the different fluorescence changes. Rather remarkably, for these derivatized proteins, the presence or absence of the fluorescence label had essentially no effect on the overall GuHCl stability (i.e., the D-PGK and D-PGK-A unfolding transitions are completely overlapping). In addition, for all the samples, the cooperativity indexes were also similar, and in the range of 10 ± 2. The overlap of all of the unfolding transitions indicates that the singly labeled donor-only sample is a good control for the doubly labeled donor/acceptor sample. The fact that the individual stabilities between different double-cysteine mutants are essentially coincident allows a direct comparison of changes in distance between different D/A pairs without having to take into account
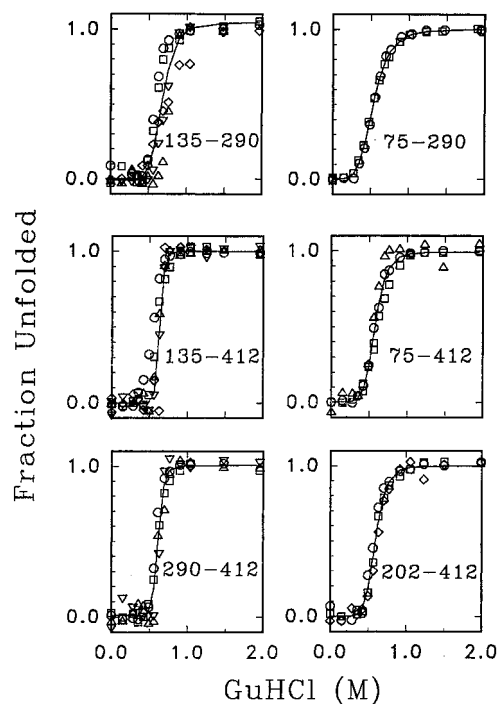
FIGURE 5: Equilibrium unfolding transitions monitored by steady-state fluorescence using multiple spectroscopic monitors (see below). The fraction of unfolded protein at each GuHCl concentration, calculated from the change in the center of mass of the emission spectra or by changes in energy-transfer efficiency, is plotted as a function of the denaturant concentration. Solid lines represent the simultaneous nonlinear least-squares fits of all the data to eq 3 using a single two-state transition: (○) tryptophan emission from D-PGK ($\lambda_{ex} = 295$ nm), (□) tryptophan emission from D-PGK-A ($\lambda_{ex} = 295$ nm), (▽) AF emission from D-PGK-A ($\lambda_{ex} = 460$ nm), (△) AEDANS emission from D-PGK ($\lambda_{ex} = 340$ nm), and (◇) fluorescence steady-state energy-transfer efficiency from the ratio of D-PGK and D-PGK-A ($\lambda_{ex} = 340$ nm, donor-side emission).

Table 4: Estimated $\langle\kappa^2\rangle^*$ Value, Maximum and Minimum κ^2 Limits, and Förster Distances for All Six Energy-Transfer Pairs

energy-transfer pair	$\langle\kappa^2\rangle^*$ (±0.2)	$\langle\kappa^2\rangle_{min}$ (±0.02)	$\langle\kappa^2\rangle_{max}$ (±0.1)	$R_o(^2/_3)$ (Å) (±1)	$R_o{}^a$ (Å) (±2)
$135 \rightarrow 290$	1.30	0.19	2.6		45.6
$290 \rightarrow 135$	1.26	0.22	2.5	43.2	50.2
$135 \rightarrow 412$	0.59	0.25	2.3		40.0
				41.9	
$412 \rightarrow 135$	0.68	0.20	2.6	42.4^b	42.6
$290 \rightarrow 412$	2.11	0.20	2.6		54.8
$412 \rightarrow 290$	2.47	0.12	3.1	43.8	52.8
$75 \rightarrow 290$	1.25	0.15	2.9		47.0
$290 \rightarrow 75$	1.24	0.14	3.0	44.0	50.1
$202 \rightarrow 412$	1.67	0.26	2.2		47.6
$412 \rightarrow 202$	2.16	0.13	3.0	41.7	51.6
$412 \rightarrow 75$	1.06	0.12	3.1	42.4	45.8

^{a} R_o from $\langle\kappa^2\rangle^*$, and J and Q_D, for each Cys, singly labeled PGK. ^{b} Specific labeled sample. All unfolded proteins were found to have a $\langle\kappa^2\rangle$ well approximated by $^2/_3$, yielding an $R_o(^2/_3)$ of 41 Å.

≈4 ns. From the measured time-resolved anisotropies of each of the probes at each of the individual sites, site-specific depolarization factors were obtained. From the measured limiting anisotropy for the fast local motion (β_g), we calculated an approximate cone angle (over which the probes move) of 35° for Cys290-, Cys412-, and Cys75-labeled positions and between 40 and 50° for Cys135, Cys202, and the unfolded proteins. Applying averaging analysis, the maximum and minimum $\langle\kappa^2\rangle_{max}$ and $\langle\kappa^2\rangle_{min}$ values from the measured depolarization factors $\langle d_D{}^x\rangle$ and $\langle d_A{}^x\rangle$ (Dale et al., 1979) were calculated. The calculated site-specific $\langle\kappa^2\rangle$ limit values are between 0.12 and 3.0 for all the different positions (Table 4). For experimental and theoretical reasons described below, this uncertainty in the $\langle\kappa^2\rangle$ value represents a large overestimation of the actual value. An improved orientation estimation procedure was also utilized, which makes use of the site-specific crystal structure, most probable fluorophore location, and measured time-resolved anisotropy mobilities [see $\langle\kappa^2\rangle^*$ (Table 4)]. Although it is very difficult to estimate, the uncertainty in the $\langle\kappa^2\rangle^*$ determined in this manner (described in detail in Materials and Methods) is approximately ±0.2. From the measured time-resolved anisotropies of the unfolded proteins (both donor- and acceptor-labeled), it is clear that $\langle\kappa^2\rangle = ^2/_3$ is a very good approximation to this state.

To experimentally test the limits of the effect of the $\langle\kappa^2\rangle$ orientation factor, as well as the lifetime heterogeneity on the recovered energy-transfer distance determination, a detailed energy-transfer study was performed on multiple specifically labeled proteins which combined sites Cys412 with Cys135. This pair represents an extreme in changes in donor orientation factor, with site Cys412 and Cys135 having donor depolarization factors ($\langle d_D{}^x\rangle$) of 0.84 and 0.64, respectively (eqs 6 and 7). This case also represents a significant change in lifetimes, in that the specifically labeled site 412 has a donor lifetime that is almost purely single-exponential (97% of a 17 ns lifetime), compared to the mixed labeled sample which consists of approximately 84% of a 17 ns component and 15% of a 5.1 ns lifetime term. The experimentally recovered intersite distances were found to be identical for these two extreme cases (Table 5; compare $135 \leftrightarrow 412$ with $412 \rightarrow 135$). Since these two independent distance measurements are performed on proteins representing an extreme in site-specific rotational mobility and altered lifetime properties, we conclude that the rotational and

altered intrinsic stability. This was a very important result which could not have been predicted beforehand; singly and doubly labeled proteins have identical (within experimental error) stabilities.

Characterization of the site-specific changes in acceptor (AF) absorption and emission (total intensity and anisotropy) was also performed (data not shown). It was found that all AF-labeled sites have nearly identical photophysical properties. There is essentially no change in the fluorescence quantum yield and molar extinction coefficient for all the different sites in the folded proteins. The absorption peak is in the range of 492−494 nm. When the protein unfolds, the emission and absorption spectra are 2−4 nm red-shifted, and the quantum yield slightly decreases from 0.8 to 0.75.

The final photophysical parameter required to completely characterize this system was the rotational characteristics of the fluorescence probes attached to each of the individual sites. Time-resolved and steady-state anisotropy experiments were performed. The steady-state anisotropies of AEDANS from each of the individual sites were 0.076 (Cys290), 0.081 (Cys412), 0.070 (Cys75), 0.047 (Cys135), and 0.053 (Cys202). In the unfolded state, all of the observed anisotropies dropped to 0.02. The time-resolved anisotropies for all of the mutants partitioned into approximately 50% fast local motion (600 ps) and 50% global motion of the entire protein (20−30 ns) (Table 3). In the unfolded state, all of the probes revealed 70% of a 600 ps motion and 30% of a slower component of

Table 5: Comparison of the Measured FRET Distances with That Predicted from the Crystal Structure[e]

| energy-transfer pair | measured steady-state distance (Å) | measured time-resolved discrete distance | | measured time-resolved distance distribution | | | crystal structure $C_\alpha \rightarrow C_\alpha$ (Å)[a] | estimated dye-to-dye distances (Å)[b] |
		R (Å)	χ^2	R_c (Å) [±2]	σ (Å)	χ^2		
135 ↔ 290	43	43.3	2.7	39.4	7.3	1.3	39	39
		40.3[c]	1.6	38.8[c]	6.1	1.2		
135 ↔ 412	40	40.4	2.7	39.5	3.8	1.3	40	46
412 → 135	40	39.5	2.1	38.0	3.9	1.2		
		38.7	1.4	38.1[c]	3.4	1.3		
290 ↔ 412	69	63.6	1.4	64.8	13.5	1.3	48	56
		56.6[c]	1.8	58.6[c]	13.2	1.4		
75 ↔ 290	50	51.7	4.3	46.6	13.5	1.2	40	46
202 ↔ 412	39	41.7	1.5	37.8	6.6	1.1	26	34
412 → 75	47	48.2	3.1	44.8	13.5	1.4	32	46
all[d]	–	60–70	1.1	60–80	15–30	1.1	–	–

[a] Watson et al. (1982). [b] Donor-to-acceptor distance from MD simulations based on Watson et al. (1982) crystal structure. [c] Acceptor-side FRET measurements. [d] Unfolded samples (MOPS buffer at pH 7.5 and 25 °C and 2 M GuHCl). [e] MOPS buffer at pH 7.5 and 25 °C. D ↔ A: average labeled samples (donor distributed between the two Cys sites). D → A: specific labeled samples. Unless otherwise indicated, distance determinations are from donor-side experiments. The errors on the recovered distances are dominated by "nonfitting" sources and are estimated to be ±3 Å (see the text).

lifetime effects on the rest of the energy-transfer pairs described in this work are probably relatively small.

Steady-State Energy Transfer. The doubly labeled PGK sample shows a major emission band due to AF fluorescence and a small contribution of AEDANS fluorescence (Figure 3, top). Donor emission is quenched through FRET from AEDANS to AF when the protein is folded. The fluorescence changes are measured by comparing the fluorescence emission spectra of the D-PGK and the D-PGK-A labeled proteins for the native samples at the same concentration. The steady-state average FRET efficiencies $\langle E \rangle$ for the native and the unfolded state are obtained from the ratio of the integrated fluorescence emission spectra of the D-PGK-A and D-PGK samples on the donor side (see Data Analysis, $\lambda_{ex} = 340$ nm, $\lambda_{em} = 400$–460 nm). Since the donor-side spectrum can be obtained over a region with absolutely no overlap with the acceptor emission, calculation of the transfer efficiencies is especially easy, and not prone to artifacts associated with spectral subtraction of the acceptor-only emission. The steady-state calculated average distances are presented in Table 5. For all the folded and unfolded samples, the scaled donor emission spectrum is subtracted from the donor/acceptor spectrum. The shape of the difference spectrum is coincident with the scaled acceptor emission spectrum that is obtained when the acceptor is excited directly ($\lambda_{ex} > 440$ nm).

AEDANS and AF fluorescence emission spectra have significant overlap. In the acceptor-side measurements ($\lambda_{em} > 480$ nm), FRET efficiencies were calculated from the AF emission enhancement (data not shown). However, due to the large number of extra manipulations of the data required to monitor the acceptor enhancement, the precision of the acceptor-determined measurements was much inferior to the donor-quench determinations. There was, however, very good agreement between the two methods, with differences in calculated energy-transfer efficiencies of ≤5%. The biggest source of error in these determinations comes from uncertainties in absolute protein concentrations and from subtraction of the directly excited acceptor emission ($\lambda_{ex} = 460$ nm).

For the unfolded samples, the differences between the D-PGK and the D-PGK-A spectra are within the experi-mental error. Time-resolved experiments (described below), however, can be performed much more accurately and allow the estimation of the intramolecular distances in the unfolded state.

Time-Resolved Energy Transfer. Time-resolved fluorescence lifetime measurements were performed on all six FRET pairs (donor side, $\lambda_{ex} = 325$ nm, $\lambda_{em} = 450$ nm). Three fluorescence lifetimes were observed for all the D-PGK decays. The fluorescence decays of D-PGK-A samples were also satisfactorily analyzed with an empirical three-expo-nential model ($\chi_g^2 = 1.1$–1.2). Analysis of the time-resolved fluorescence data was performed at three different levels of complexity: (1) average energy-transfer efficiency calculated from the mean lifetime of donor and donor/acceptor proteins, (2) global analysis of donor and donor/acceptor decay in terms of discrete distance(s), and (3) global analysis of donor and donor/acceptor decay in terms of a distribution of distances.

The first level of analysis of the time-resolved data was analysis of the D-PGK and D-PGK-A fluorescence decays in terms of empirical exponential functions. From these recovered lifetimes (see Materials and Methods), one can calculate energy-transfer efficiencies using $E = 1 - (\langle\tau_{DA}\rangle/\langle\tau_D\rangle)$. The main purpose of this analysis was simply to determine if the steady-state transfer efficiencies and time-resolved data were internally consistent. Since the time-resolved data did not require knowledge of the absolute concentrations of the donor-only and donor/acceptor samples, uncertainties in protein concentrations would not contribute to a measured efficiency. Similarly, the steady-state transfer efficiencies can be affected by static quenching mechanisms which will not affect the time-resolved signals. When the data analysis is performed in this very simple manner, one finds that the recovered distances determined by both methods are in complete agreement (see Table 5). These results support the accuracy of both the protein concentration determination of each of the mutants and the fact that the majority (if not all) of the donor quenching which is observed in the steady-state measurement is dynamic in nature and consistent with an energy-transfer process. It should be noted that the small amplitude (<1% of total fluorescence) short

lifetime component was invariant between donor and donor/acceptor samples and hence does not appear to be undergoing any fluorescence energy transfer. Therefore, in all of our subsequent analyses, no energy-transfer distance was associated with this short lifetime term and its value was linked between both the donor-only and donor/acceptor samples.

Global analyses were then performed by simultaneously analyzing the decay curves of the D-PGK and D-PGK-A samples in terms of an internally consistent distance(s). Both discrete and distributed distances (parameterized as Gaussians) were utilized. Global fits in terms of a single discrete distance were not satisfactory for any of the native proteins. Severe distortions in the weighted residual distribution were apparent, and the reduced χ_g^2 values for most of these analyses were >2.0. Global analysis of the time-resolved energy-transfer data in terms of a single distributed distance yielded the best χ_g^2 and random residual patterns with the least number of adjustable fitting parameters. Protein conformational heterogeneity, orientational factor, and the length and flexibility of the linker of the donor and acceptor probes may be contributing to this distribution. The global fitting in terms of a Gaussian distance distribution gave a satisfactory fit to the data for all six donor/acceptor pairs. Random residual patterns (such as those shown in Figure 3, bottom) and reduced global χ_g^2 values in the range of 1.1−1.3 were obtained for all cases. The mean distance from the single-distance distribution analysis, R_c, was in good agreement with the corresponding discrete single-distance analysis.

Three of the six energy-transfer pairs were also examined by global analysis of data obtained at the acceptor-side emission, with excitation at 325 nm and emission at 560 nm (Table 5). Nearly identical distance distributions are obtained from the acceptor-side fluorescence emission, further strengthening the fact that the observed quenching in this system is dominated by energy transfer and not some other mechanism. For the unfolded proteins (2 M GuHCl), only small energy-transfer efficiencies are observed. Since the transfer efficiencies are rather small, it is not possible to perform the sophisticated type of distribution analysis which is performed for the native proteins. The global analyses were consistent with either a single discrete distance model or a broad distribution distance model. All of the energy-transfer signals are reversible, as refolded proteins were found to have distance distributions nearly identical to those of proteins which were never previously unfolded.

Figure 6 shows the recovered donor−acceptor distance distributions of all six doubly labeled PGK derivatives. The mean of the recovered donor−acceptor distance distribution matches that predicted from the crystal structure almost exactly for 75 ↔ 290, 412 → 75, 202 ↔ 412, and 135 ↔ 290. These four sites span quite different regions of the tertiary structure of PGK (for donor/acceptor pair locations, refer to Figure 1). For 290 ↔ 412, the recovered mean from the donor-side decay is 65 Å, while the predicted dye-to-dye distance is 56 Å. The acceptor-side measurements yielded a distance of 59 Å, much closer to the predicted distance for this case. The recovered mean distance from 135 ↔ 412 and 412 → 135 is 40 Å (compared to a predicted separation distance of 46 Å) when measured from either donor quench or acceptor enhancement (three independent measurements, two different samples). Given the identical
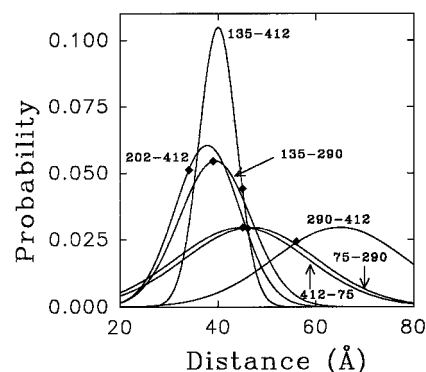

FIGURE 6: Recovered energy-transfer distance distributions from the global analysis of the time-resolved fluorescence decays of D-PGK and D-PGK-A. The orientation factor $\langle\kappa^2\rangle^*$ was utilized for each analysis. The predicted dye-to-dye distances (◆) from the molecular dynamics simulation of each dye pair built into the PGK crystal structure are shown for comparison.
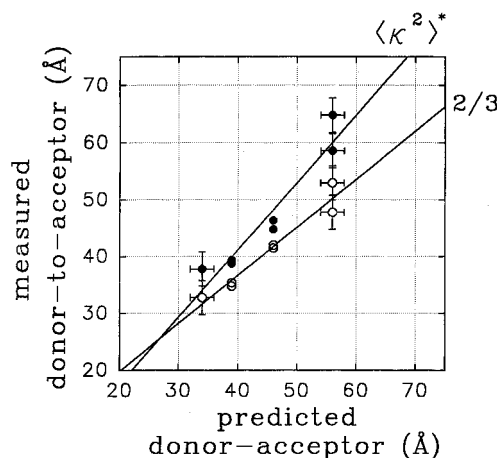

FIGURE 7: Linear correlation of the measured energy-transfer distances (mean of the recovered distribution function) as a function of the predicted dye-to-dye distance from the molecular dynamics simulation of each dye pair built into the PGK crystal structure. The regression line and data for both the $\langle\kappa^2\rangle = 2/3$ and the enhanced orientation factor estimation $\langle\kappa^2\rangle^*$ are shown. A "perfect" distance assay would be a line extending exactly along the diagonal.

energy-transfer distances which are obtained at this position, it is entirely possible that the majority of the "error" associated with this site has to do with the calculation of the projected dye-to-dye separation distance.

A plot of the recovered energy-transfer distances as a function of predicted dye-to-dye distances (using the PGK crystal structure) is shown in Figure 7. Independent of the $\langle\kappa^2\rangle$ or type of data (time-resolved or steady-state fluorescence), linear correlations are observed for the recovered distances versus predicted distances from the crystal structure. The correlation coefficients for these lines are 0.97 and 0.96 for the time-resolved $\langle\kappa^2\rangle$ (=2/3) and the $\langle\kappa^2\rangle^*$ respectively. The slope of the linear regression line of the time-resolved energy-transfer distance estimations with $\langle\kappa^2\rangle^*$ is 1.18, and with $\langle\kappa^2\rangle$ (=2/3) 0.85. This result compares very favorably with the ideal-case distance assay which would have a slope of 1.0, indicating that, for all of the donor/acceptor probes (when examined as a total system), the measured distances reflect the predicted structural distances to within <20%. For these regression curves, the 135 ↔ 412 energy-transfer pair was omitted due to probable errors in the calculation of the predicted dye-to-dye distance (see above). However, even when this additional FRET pair is included, the

correlation coefficient is still very good ($r = 0.89$), and the slope is 1.16.

CONCLUSIONS

The determination of long-range distance changes in proteins ($10-100$ Å) is an area that only fluorescence energy-transfer measurements (FRET) are currently capable of making. This work represents the first case study in which six independent donor/acceptor pairs have been engineered into a single protein for the expressed purpose of making distance measurements during a protein folding reaction. Essential for this study were the determinations that the fluorescence probes (themselves) did not alter the folding reaction and that the FRET assay was dominated by changes in distance and not by some other spectroscopic effect.

A systematic investigation of (up to) nine singly and doubly labeled proteins at each of the six donor/acceptor sites was able to conclusively show that the stabilities of each of the labeled proteins were identical (Figure 5 and Table 2). This was not exactly an expected result, in that it would be very easy to imagine that the inherent stability of the doubly labeled PGK would differ from that of the singly labeled protein. There are, however, cysteine sites in PGK where this strategy will not work (e.g., the native Cys97; data not shown) where the stability of the protein labeled at this site is dramatically altered. In these studies, we have avoided all sites with altered stability characteristics. We have found that these "extra-sensitive sites" are in a minority and that, by using the crystal structure as a guide, cysteine sites can often be engineered into a protein and labeled with fluorophores without producing a significant perturbation in stability.

A variety of spectroscopic effects could (in theory) dominate the energy-transfer efficiencies which are measured in a native (or partially folded) structure. Therefore it was absolutely imperative to show that the recovered energy-transfer distances correlated with distances predicted from the crystal structure of PGK. Figures 6 and 7 reveal that, over the measured distance range of $30-70$ Å, the multisite distance assay which has been engineered into PGK accurately measures the distances predicted from the crystal structure to within 20%. Examination of Figure 1 reveals that this distance assay system will be capable of quantitating long-range distance changes between the amino and carboxyl-terminal domains, within the amino-terminal domain, as well as "unraveling" of the C-terminal end from the amino-terminal domain. The use of this multisite FRET-based distance assay to monitor the kinetics of unfolding of PGK is described in the following paper.

ACKNOWLEDGMENT

REFERENCES

Beechem, J. M., Gratton, E., Ameloot, M., Knutson, J. R., & Brand, L. (1991) in *Topics in Fluorescence Spectroscopy: Principles II* (Lakowicz, J. R., Ed.) pp 241−305, Plenum Press, New York.

Beechem, J. M., Sherman, M. A., & Mas, M. T. (1995) *Biochemistry 34*, 13943−13948.

Bloom, L. B., Otto, M. R., Eritja, R., Reha-Krantz, L. J., Goodman, M. F., & Beechem, J. M. (1994) *Biochemistry 33*, 7576−7586.

Bradford, M. M. (1976) *Anal. Biochem. 72*, 248−254.

Chantler, P. D., & Tao, T. (1986) *J. Mol. Biol. 192*, 87−89.

Chen, E. Y., & Seeburg, P. H. (1985) *DNA 4*, 165−170.

Chen, R. F., & Bowman, R. L. (1965) *Science 147*, 729−732.

Dale, R. E., & Eisinger, J. (1975) in *Biochemical Fluorescence*: Concepts (Chen, R. F., & Edelhoch, H., Eds.) Vol. 1, pp 115−284, Marcel Dekker, Inc., New York.

Dale, R. E., Eisinger, J., & Blumberg, W. E. (1979) *Biophys. J. 26*, 161−194.

Gill, S. C., & von Hippel, P. H. (1989) *Anal. Biochem. 182*, 319−326.

Haas, E., & Steinberg, I. Z. (1984) *Biophys. J. 46*, 429−437.

Haas, E., & Beechem, J. M. (1989) *Biophys. J. 55*, 1225−1236.

Haas, E., Katchalski-Katzir, E., & Steinberg, I. Z. (1978) *Biopolymers 17*, 11−31.

Haas, E., McWherter, C. A., & Scheraga, H. A. (1988) *Biopolymers 27*, 1−21.

Haran, G., Haas, E., Szpikowska, B. K., & Mas, M. T. (1992) *Proc. Natl. Acad. Sci. U.S.A. 89*, 11764−11768.

Hudson, E. N., & Weber, G. (1973) *Biochemistry 12*, 4154−4161.

Jones, B. J., Beechem, J. M., & Matthews, C. R. (1995) *Biochemistry 34*, 1867−1877.

Kinosita, K., Kawato, S., & Ikegami, A. (1977) *Biophys. J. 20*, 289−305.

Lillo, M. P., Szpikowska, B. K., Mas, M. T., Sutin, J. D., & Beechem, J. M. (1997) *Biochemistry 36*, 11273−11281.

Mas, M. T., Chen, C. Y., Hitzeman, R. A., & Riggs, A. D. (1986) *Science 233*, 788−790.

Mayo, S. L., Olafson, B. D., & Goddard, W. A., III (1990) J. Phys. Chem. 94, 8897−8909.

Nozaki, Y. (1972) in *Methods in Enzymology* (Hirs, C. H. W., & Timasheff, S. N., Eds.) Vol. 26, p 23, Academic Press, New York.

Pace, C. N., Shirley, B. A., & Thomson, J. A. (1989) in *Protein Structure: A practical approach* (Creighton, T. E., Ed.) pp 311−330, IRL Press, Oxford, UK.

Sherman, M. A., Szpikowska, B. K., Dean, S. A., Mathiowetz, A. M., McQueen, N. L., & Mas, M. T. (1990) *J. Biol. Chem. 265*, 10659−10665.

Sherman, M. A., Beechem, J. M., & Mas, M. T. (1995) *Biochemistry 34*, 13924−13942.

Szpikowska, B. K., Beechem, J. M., Sherman, M. A., & Mas, M. T. (1994) *Biochemistry 33*, 2217−2225.

Van de Meer, B. W., Cooker, G., III, & Chen, S. Y. (1994) in *Resonance Energy Transfer. Theory and data*, p 150, VCH Publishers, Inc.

Velapoldi, R. A. (1972) *J. Res. Natl. Bur. Stand. (U. S.) 76A*, 641−654.

Watson, H. C., Walker, N. P. C., Shaw, P. J., Bryant, T. N., Wendell, P. L., Fothergill, L. A., Perkins, R. E., Conroy, S. C., Dobson, M., Tuite, M. F., Kingsman, A. J., & Kingsman, S. M. (1982) *EMBO J. 1*, 1635−1640.